INTERNATIONAL JOURNAL FOR NUMERICAL METHODS IN FLUIDS
Int. J. Numer. Meth. Fluids 2010; **64**:549–564
Published online 15 September 2009 in Wiley Online Library (wileyonlinelibrary.com). DOI: 10.1002/fld.2161

Discontinuous Galerkin methods for the Navier–Stokes equations using solenoidal approximations

A. Montlaur[1,2], S. Fernandez-Mendez[1,3], J. Peraire[4] and A. Huerta[1,3,*,†]

[1]*Laboratori de Càlcul Numèric* (*LaCàN*), *Universitat Politècnica de Catalunya*, *Jordi Girona 1-3*, *08034 Barcelona*, *Spain*
[2]*Escola Politècnica Superior de Castelldefels*, *Spain*
[3]*Departament de Matematica Aplicada III*, *E.T.S. Ingenieros de Caminos*, *Barcelona*, *Spain*
[4]*Aerospace Computational Design Laboratory*, *Department of Aeronautics and Astronautics*, *Massachusetts Institute of Technology*, *Cambridge*, *MA 02139*, *U.S.A.*

SUMMARY

An interior penalty method and a compact discontinuous Galerkin method are proposed and compared for the solution of the steady incompressible Navier–Stokes equations. Both compact formulations can be easily applied using high-order piecewise divergence-free approximations, leading to two uncoupled problems: one associated with velocity and hybrid pressure, and the other one only concerned with the computation of pressures in the elements interior. Numerical examples compare the efficiency and the accuracy of both proposed methods. Copyright © 2009 John Wiley & Sons, Ltd.

Received 26 February 2009; Revised 7 July 2009; Accepted 18 July 2009

KEY WORDS: compact discontinuous Galerkin; interior penalty method; Navier–Stokes; high order; solenoidal; incompressible; hybrid pressure

1. INTRODUCTION

Recently, several authors have focused their attention on discontinuous Galerkin (DG) formulations for computational fluid dynamics [1], and in particular for incompressible flow. Divergence-free high-order approximations are easily defined within a DG framework for incompressible problems. Namely, a divergence-free polynomial basis is considered in each element. The divergence-free approach induces an important decrement in the number of degrees of freedom (dof) with the

*Correspondence to: A. Huerta, Departament de Matemàtica Aplicada III, E.T.S. Ingenieros de Caminos, Universitat Politècnica de Catalunya, Jordi Girona 1, E-08034 Barcelona, Spain.
†E-mail: antonio.huerta@upc.edu

Contract/grant sponsor: Ministerio de Educación y Ciencia; contract/grant numbers: BIA2007-66965, DPI2007-62395
Contract/grant sponsor: Generalitat de Catalunya AGAUR; contract/grant number: 2005SGR917

corresponding reduction in computational cost. Following this idea, in [2–6] Stokes equations are solved using a decomposition of the approximation space for the velocity field as direct sum of a solenoidal space and an irrotational space. This allows to split the DG weak form into two uncoupled problems: the first one solves for velocities and hybrid pressures (pressure along the mesh sides/faces) and the second one allows the computation of pressure in the interior of the elements.

Many DG methods have recently been developed in the framework of computational fluid dynamics, such as the local discontinuous Galerkin (LDG) method [7], the compact discontinuous Galerkin (CDG) method [8], or the interior penalty method (IPM) [6]. LDG proposes a mixed formulation with vorticity, velocity, and pressure. Lifting operators are introduced to substitute vorticity, thus leading to a velocity–pressure formulation. LDG has been successfully analyzed and applied to Stokes, Oseen, and Navier–Stokes equations, see for instance [7]. However, one major drawback of LDG is the loss of compactness due to the introduction of lifting factors. That is, the LDG stencil goes beyond immediate neighbors, in front of the usual DG stencil where dof in one element are connected only to those in the neighboring elements. To avoid this loss of compactness, CDG was introduced in [8] with application to elliptic problems. CDG is very similar to LDG, but it eliminates coupling between the dof of non-neighboring elements by means of alternative local lifting operators. Another possible compact formulation is obtained when using an IPM, which was first introduced by Arnold [9] for second-order parabolic equations. An IPM with piecewise solenoidal approximation is proposed for the solution of incompressible Stokes equations in [6].

IPM and CDG have many points in common, both methods inducing compact formulations and leading to symmetric and coercive bilinear forms for self-adjoint operators. Nevertheless, one of the most remarkable differences is that the IPM formulation does not involve lifting operators, leading to a much simpler and straightforward implementation, with a non-negligible reduction in the computational cost. To further compare these methods, IPM and CDG formulations are derived in this paper for the solution of the incompressible Navier–Stokes equations. For IPM, the rationale proposed in [6] in the context of Stokes equations is extended to Navier–Stokes equations. The CDG formulation is derived following the basis of the method for elliptic problems presented in [8]. Both compact formulations can be easily applied using high-order piecewise divergence-free approximations.

The contributions of this paper are presented as follows. The DG formulations for the solution of the incompressible Navier–Stokes equations, with Dirichlet and Neumann boundary conditions, are presented in Section 2.2 for IPM, and in Section 2.3 for CDG. Particularization of the two weak forms with a splitting of the velocity space into solenoidal and irrotational parts is detailed in Section 2.4. Numerical tests show the applicability of both methodologies (IPM and CDG) and compare their accuracy in Section 3.

2. THE NAVIER–STOKES PROBLEM AND TWO ALTERNATIVE FORMULATIONS

2.1. Problem statement and definitions

Let $\Omega \subset \mathbb{R}^{\mathtt{n_{sd}}}$ be an open bounded domain with boundary $\partial\Omega$, and $\mathtt{n_{sd}}$ the number of spatial dimensions. The strong form for the homogeneous steady incompressible Navier–Stokes problem

DOI: 10.1002/fld

can be written as

$$-2\boldsymbol{\nabla}\cdot(\nu\boldsymbol{\nabla}^{\mathrm{s}}\mathbf{u})+\boldsymbol{\nabla}p+(\mathbf{u}\cdot\boldsymbol{\nabla})\mathbf{u}=\mathbf{f}\quad\text{in }\Omega \tag{1a}$$

$$\boldsymbol{\nabla}\cdot\mathbf{u}=0\quad\text{in }\Omega \tag{1b}$$

$$\mathbf{u}=\mathbf{u}_{\mathrm{D}}\quad\text{on }\Gamma_{\mathrm{D}} \tag{1c}$$

$$-p\mathbf{n}+2\nu(\mathbf{n}\cdot\boldsymbol{\nabla}^{\mathrm{s}})\mathbf{u}=\mathbf{t}\quad\text{on }\Gamma_{\mathrm{N}} \tag{1d}$$

where $\partial\Omega=\overline{\Gamma}_{\mathrm{D}}\cup\overline{\Gamma}_{\mathrm{N}}$, $\Gamma_{\mathrm{D}}\cap\Gamma_{\mathrm{N}}=\emptyset$, $\mathbf{f}\in\mathscr{L}_2(\Omega)$ is a source term, $\mathbf{u}$ is the flux velocity, and p its pressure, ν is the kinematic viscosity, $\mathbf{n}$ is the exterior unit normal vector, and $\boldsymbol{\nabla}^{\mathrm{s}}=\frac{1}{2}(\boldsymbol{\nabla}+\boldsymbol{\nabla}^{\mathrm{T}})$. In (1a), the constant density has been absorbed into the pressure.

Moreover, suppose that Ω is partitioned into $\mathtt{n_{el}}$ disjoint subdomains Ω_i

$$\overline{\Omega}=\bigcup_{i=1}^{\mathtt{n_{el}}}\overline{\Omega}_i,\quad \Omega_i\cap\Omega_j=\emptyset\quad\text{for } i\neq j$$

with piecewise linear boundaries $\partial\Omega_i$, which define an internal interphase Γ

$$\Gamma:=\left[\bigcup_{i=1}^{\mathtt{n_{el}}}\partial\Omega_i\right]\Big\backslash\,\partial\Omega$$

The *jump* $[\![\cdot]\!]$ and *mean* $\{\cdot\}$ operators are defined along the interface Γ using values from the elements to the left and to the right of the interface (say, Ω_i and Ω_j) and are also extended along the exterior boundary (only values in Ω are employed), namely

$$[\![\circledcirc]\!]=\begin{cases}\circledcirc_i+\circledcirc_j & \text{on }\Gamma\\ \circledcirc & \text{on }\partial\Omega\end{cases}\quad\text{and}\quad\{\circledcirc\}=\begin{cases}\kappa_i\circledcirc_i+\kappa_j\circledcirc_j & \text{on }\Gamma\\ \circledcirc & \text{on }\partial\Omega\end{cases}$$

Usually, $\kappa_i=\kappa_j=\frac{1}{2}$ but, in general, these two scalars are only required to verify $\kappa_i+\kappa_j=1$, see for instance [10]. The major difference between the mean and the jump operator is that the latter always involves the normal to the interface or to the domain. For instance, given two contiguous subdomains Ω_i and Ω_j their exterior unit normals are denoted, respectively, as $\mathbf{n}_i$ and $\mathbf{n}_j$ (recall that $\mathbf{n}_i=-\mathbf{n}_j$) and along $\partial\Omega$ the exterior unit normal is denoted by $\mathbf{n}$; the jump is then

$$[\![p\,\mathbf{n}]\!]=\begin{cases}p_i\mathbf{n}_i+p_j\,\mathbf{n}_j=\mathbf{n}_i(p_i-p_j) & \text{on }\Gamma\\ p\mathbf{n} & \text{on }\partial\Omega\end{cases}$$

for scalars, see [6] for vectors or tensors.

The following discrete finite element spaces are also introduced:

$$\mathscr{V}^h=\{\mathbf{v}\in[\mathscr{L}_2(\Omega)]^{\mathtt{n_{sd}}};\,\mathbf{v}|_{\Omega_i}\in[\mathscr{P}^k(\Omega_i)]^{\mathtt{n_{sd}}}\ \forall\Omega_i\}$$

$$\mathscr{Q}^h=\{q\in[\mathscr{L}_2(\Omega)];\,q|_{\Omega_i}\in[\mathscr{P}^{k-1}(\Omega_i)]\ \forall\Omega_i\}$$

where $\mathscr{P}^k(\Omega_i)$ is the space of polynomial functions of degree at most $k\geqslant 1$ in Ω_i.

Finally, in the following equations, $(\cdot,\cdot)$ denotes the $\mathscr{L}_2$ scalar product in Ω, that is

$$(p,q)=\int_\Omega pq\,\mathrm{d}\Omega\quad\text{for scalars}$$

DOI: 10.1002/fld

$$(\mathbf{u},\mathbf{v})=\int_\Omega \mathbf{u}\cdot\mathbf{v}\,\mathrm{d}\Omega \quad \text{for vectors}$$

$$(\boldsymbol{\sigma},\boldsymbol{\tau})=\int_\Omega \boldsymbol{\sigma}:\boldsymbol{\tau}\,\mathrm{d}\Omega \quad \text{for second-order tensors}$$

Analogously, $(\cdot,\cdot)_\Upsilon$ denotes the $\mathscr{L}_2$ scalar product in any domain $\Upsilon\subset\Gamma\cup\partial\Omega$. For instance,

$$(p,q)_\Upsilon=\int_\Upsilon pq\,\mathrm{d}\Gamma$$

for scalars.

2.2. IPM formulation

Here, the interior penalty approach presented in [6] for the Stokes equations is extended to the Navier–Stokes equations. The weak form containing the nonlinear convection becomes, find $\mathbf{u}_h\in\mathscr{V}^h$ and $p_h\in\mathscr{Q}^h$ such that

$$\begin{aligned} a_{\mathtt{IP}}(\mathbf{u}_h,\mathbf{v})+c(\mathbf{u}_h;\mathbf{u}_h,\mathbf{v})+b(\mathbf{v},p_h)+(\{p_h\},[\![\mathbf{n}\cdot\mathbf{v}]\!])_{\Gamma\cup\Gamma_\mathrm{D}}&=l_{\mathtt{IP}}(\mathbf{v}) \quad \forall\mathbf{v}\in\mathscr{V}^h\\ b(\mathbf{u}_h,q)+(\{q\},[\![\mathbf{n}\cdot\mathbf{u}_h]\!])_{\Gamma\cup\Gamma_\mathrm{D}}&=(q,\mathbf{n}\cdot\mathbf{u}_\mathrm{D})_{\Gamma_\mathrm{D}} \quad \forall q\in\mathscr{Q}^h \end{aligned} \tag{2}$$

where the following forms must be defined:

$$\begin{aligned} a_{\mathtt{IP}}(\mathbf{u},\mathbf{v}):=&(2\nu\nabla^\mathrm{S}\mathbf{u},\nabla^\mathrm{S}\mathbf{v})+C_{11}([\![\mathbf{n}\otimes\mathbf{u}]\!],[\![\mathbf{n}\otimes\mathbf{v}]\!])_{\Gamma\cup\Gamma_\mathrm{D}}\\ &-(2\nu\{\nabla^\mathrm{S}\mathbf{u}\},[\![\mathbf{n}\otimes\mathbf{v}]\!])_{\Gamma\cup\Gamma_\mathrm{D}}-([\![\mathbf{n}\otimes\mathbf{u}]\!],2\nu\{\nabla^\mathrm{S}\mathbf{v}\})_{\Gamma\cup\Gamma_\mathrm{D}} \end{aligned} \tag{3a}$$

$$l_{\mathtt{IP}}(\mathbf{v}):=(\mathbf{f},\mathbf{v})+(\mathbf{t},\mathbf{v})_{\Gamma_\mathrm{N}}+C_{11}(\mathbf{u}_\mathrm{D},\mathbf{v})_{\Gamma_\mathrm{D}}-(\mathbf{n}\otimes\mathbf{u}_\mathrm{D},2\nu\nabla^\mathrm{S}\mathbf{v})_{\Gamma_\mathrm{D}} \tag{3b}$$

$$\begin{aligned} c(\mathbf{w};\mathbf{u},\mathbf{v}):=&-((\mathbf{w}\cdot\nabla)\mathbf{v},\mathbf{u})+\sum_{i=1}^{\mathtt{n_{el}}}\int_{\partial\Omega_i\setminus\Gamma_\mathrm{N}}\frac{1}{2}[(\mathbf{w}\cdot\mathbf{n}_i)(\mathbf{u}^{\mathrm{ext}}+\mathbf{u})-|\mathbf{w}\cdot\mathbf{n}_i|(\mathbf{u}^{\mathrm{ext}}-\mathbf{u})]\cdot\mathbf{v}\,\mathrm{d}\Gamma\\ &+\int_{\Gamma_\mathrm{N}}(\mathbf{w}\cdot\mathbf{n})\mathbf{u}\cdot\mathbf{v}\,\mathrm{d}\Gamma \end{aligned} \tag{4a}$$

and

$$b(\mathbf{v},p):=-\int_\Omega q\nabla\cdot\mathbf{v}\,\mathrm{d}\Omega \tag{4b}$$

The penalty parameter, a positive scalar C_{11} of order $\mathcal{O}(h^{-1})$, must be large enough to ensure coercivity of the bilinear form $a_{\mathtt{IP}}(\cdot,\cdot)$, see [6]. The characteristic mesh size is denoted by h. A standard upwind numerical flux, see for instance [11], is used for the definition of the convective term $c(\cdot;\cdot,\cdot)$. In (4a), $\mathbf{u}^{\mathrm{ext}}$ denotes the exterior trace of $\mathbf{u}$ taken over the side/face under consideration, that is

$$\mathbf{u}^{\mathrm{ext}}(\mathbf{x})=\lim_{\varepsilon\to0^+}\mathbf{u}(\mathbf{x}+\varepsilon\mathbf{n}_i) \quad \text{for } \mathbf{x}\in\partial\Omega_i$$

DOI: 10.1002/fld

2.3. CDG formulation

This section shows the application of CDG to the solution of the Navier–Stokes equations. As usual in CDG [8], two local lifting operators are defined on interior and Dirichlet sides/faces. For $\Gamma_e \subset \Gamma \cup \Gamma_D$, the lifting $r^e : [\mathscr{L}_2(\Gamma_e)]^{n_{sd}^2} \to \boldsymbol{\Sigma}^h$ is defined by

$$\int_\Omega r^e(\boldsymbol{\sigma}) : \boldsymbol{\tau} \, d\Omega = \int_{\Gamma_e} \boldsymbol{\sigma} : \{\boldsymbol{\tau}\} \, d\Gamma \quad \forall \boldsymbol{\tau} \in \boldsymbol{\Sigma}^h \tag{5}$$

where $\boldsymbol{\Sigma}^h = \boldsymbol{\nabla}^s \boldsymbol{\mathscr{V}}^h$. The second lifting, $s^e : [\mathscr{L}_2(\Gamma_e)]^{n_{sd}} \to \boldsymbol{\Sigma}^h$, is such that $s^e(\mathbf{v}) = \mathbf{0} \ \forall \mathbf{v} \in [\mathscr{L}_2(\Gamma_e)]^{n_{sd}}$ for $\Gamma_e \subset \Gamma_D$, and is defined by

$$\int_\Omega s^e(\mathbf{v}) : \boldsymbol{\tau} \, d\Omega = \int_{\Gamma_e} \mathbf{v} \cdot [\![\mathbf{n} \cdot \boldsymbol{\tau}]\!] \, d\Gamma \quad \forall \boldsymbol{\tau} \in \boldsymbol{\Sigma}^h$$

for all interior sides $\Gamma_e \subset \Gamma$.

The extension of CDG to Navier–Stokes equations combines the rationale detailed in [8] for the second-order differential operators and the one proposed in [7, 12] for the first-order ones. The CDG scheme becomes: find $\mathbf{u}_h \in \boldsymbol{\mathscr{V}}^h$ and $p_h \in \mathscr{Q}^h$ such that

$$\begin{aligned} a_{CDG}(\mathbf{u}_h, \mathbf{v}) + c(\mathbf{u}_h; \mathbf{u}_h, \mathbf{v}) + b(\mathbf{v}, p_h) + (\{p_h\}, [\![\mathbf{n} \cdot \mathbf{v}]\!])_{\Gamma \cup \Gamma_D} &= l_{CDG}(\mathbf{v}) \quad \forall \mathbf{v} \in \boldsymbol{\mathscr{V}}^h \\ b(\mathbf{u}_h, q) + (\{q\}, [\![\mathbf{n} \cdot \mathbf{u}_h]\!])_{\Gamma \cup \Gamma_D} &= (q, \mathbf{n} \cdot \mathbf{u}_D)_{\Gamma_D} \quad \forall q \in \mathscr{Q}^h \end{aligned} \tag{6}$$

where the forms $c(\cdot;\cdot,\cdot)$ and $b(\cdot,\cdot)$ are already defined in (4), and the two new forms are

$$\begin{aligned} a_{CDG}(\mathbf{u}, \mathbf{v}) := a_{IP}(\mathbf{u}, \mathbf{v}) &- (2\nu \mathbf{C}_{12} \otimes [\![\mathbf{n} \cdot \boldsymbol{\nabla}^s \mathbf{v}]\!], [\![\mathbf{n} \otimes \mathbf{u}]\!])_\Gamma - (2\nu \mathbf{C}_{12} \otimes [\![\mathbf{n} \cdot \boldsymbol{\nabla}^s \mathbf{u}]\!], [\![\mathbf{n} \otimes \mathbf{v}]\!])_\Gamma \\ &+ \sum_{\Gamma_e \subset \Gamma \cup \Gamma_D} (2\nu (r^e([\![\mathbf{n} \otimes \mathbf{u}]\!]) + s^e(\mathbf{C}_{12} \cdot [\![\mathbf{n} \otimes \mathbf{u}]\!])), r^e([\![\mathbf{n} \otimes \mathbf{v}]\!]) + s^e(\mathbf{C}_{12} \cdot [\![\mathbf{n} \otimes \mathbf{v}]\!])) \end{aligned} \tag{7a}$$

$$l_{CDG}(\mathbf{v}) := l_{IP}(\mathbf{v}) + \sum_{\Gamma_e \subset \Gamma_D} (2\nu r^e(\mathbf{n} \otimes \mathbf{v}), r^e(\mathbf{n} \otimes \mathbf{u}_D)) \tag{7b}$$

being $a_{IP}(\cdot,\cdot)$ and $l_{IP}(\cdot)$ the IPM forms defined in (3). The CDG forms have two parameters, C_{11} and $\mathbf{C}_{12}$. The former, C_{11}, as in IPM, is a non-negative parameter of order $\mathcal{O}(h^{-1})$. The latter is an additional vector, $\mathbf{C}_{12} \in \mathbb{R}^{n_{sd}}$, which is defined for each interior side/face of the domain according to

$$\mathbf{C}_{12} = \tfrac{1}{2}(S_{ij}\mathbf{n}_i + S_{ji}\mathbf{n}_j)$$

where $S_{ij} \in \{0, 1\}$ denotes the switch associated with element Ω_i on the side/face that element Ω_i shares with element Ω_j. There are several possible choices of the switches, always satisfying $S_{ij} + S_{ji} = 1$, see [8, 13] for details.

Remark 1

In CDG, $C_{11} = 0$ may be considered on Γ, see [8]. However, on the Dirichlet boundary it must be positive, $C_{11} > 0$, to treat properly boundary conditions.

Remark 2

Lifting operators in CDG are associated with individual sides/faces, and therefore there are no connectivities between non-neighbor elements. This is also the case for IPM, but not for LDG,

DOI: 10.1002/fld

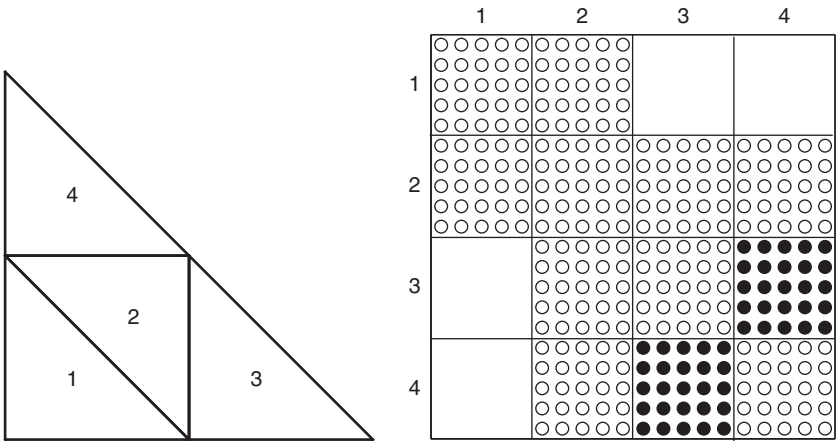

Figure 1. Sparsity structure of the diffusion matrix for four triangles with quadratic velocity. IPM and CDG (○) are both compact in the sense that they only connect neighboring triangles, whereas LDG (○ and ●) is non-compact and connects some non-neighboring triangles (3 and 4).

see [8], as it can be seen in Figure 1. IPM and CDG never connect non-neighboring elements, whereas LDG may connect some non-neighboring elements.

Remark 3

It is worth noticing that the CDG weak form can be written as the IPM weak form plus some extra terms, mainly involving CDG lifting operators, see Equations (6) and (7). The implementation of these extra lifting terms in CDG requires computing several elemental matrices, matrix inversions and products, for every side/face (see Appendix A). Thus, in addition to the implementation effort, lifting terms represent a clearly non-negligible increase in the computational cost relative to IPM. This is also the case for unsteady problems and implies a non-negligible burden mostly for explicit time integrators. Auxiliary variables for the liftings have to be stored and computed (solving linear systems of equations in each element) at every time step.

2.4. DG formulations with solenoidal approximations

Following [2–4, 6], the velocity space $\mathscr{V}^h$ is split into the direct sum of a solenoidal part and an irrotational part $\mathscr{V}^h = \mathscr{S}^h \oplus \mathscr{I}^h$, where

$$\mathscr{S}^h = \{\mathbf{v} \in [\mathscr{H}^1(\Omega)]^{\mathtt{n_{sd}}} \,|\, \mathbf{v}|_{\Omega_i} \in [\mathscr{P}^k(\Omega_i)]^{\mathtt{n_{sd}}}, \nabla \cdot \mathbf{v}|_{\Omega_i} = 0 \text{ for } i = 1, \ldots, \mathtt{n_{el}}\}$$

$$\mathscr{I}^h \subset \{\mathbf{v} \in [\mathscr{H}^1(\Omega)]^{\mathtt{n_{sd}}} \,|\, \mathbf{v}|_{\Omega_i} \in [\mathscr{P}^k(\Omega_i)]^{\mathtt{n_{sd}}}, \nabla \times \mathbf{v}|_{\Omega_i} = \mathbf{0} \text{ for } i = 1, \ldots, \mathtt{n_{el}}\}$$

For instance, a solenoidal basis in a 2D triangle for an approximation of degree $k = 2$ is

$$\mathscr{S}^h = \left\langle \begin{pmatrix} 1 \\ 0 \end{pmatrix}, \begin{pmatrix} 0 \\ 1 \end{pmatrix}, \begin{pmatrix} 0 \\ x \end{pmatrix}, \begin{pmatrix} x \\ -y \end{pmatrix}, \begin{pmatrix} y \\ 0 \end{pmatrix}, \begin{pmatrix} 0 \\ x^2 \end{pmatrix}, \begin{pmatrix} 2xy \\ -y^2 \end{pmatrix}, \begin{pmatrix} x^2 \\ -2xy \end{pmatrix}, \begin{pmatrix} y^2 \\ 0 \end{pmatrix} \right\rangle \tag{8}$$

DOI: 10.1002/fld

and an irrotational basis for $k=2$ is

$$\mathscr{J}^h=\left\langle \begin{pmatrix} x \\ 0 \end{pmatrix}, \begin{pmatrix} x^2 \\ 0 \end{pmatrix}, \begin{pmatrix} 0 \\ y^2 \end{pmatrix} \right\rangle$$

see for example [3] for the construction of these bases.

Under these circumstances, the IPM problem (2) can be split into two *uncoupled* problems. The first one solves for *divergence-free* velocities and *hybrid pressures*: find $\mathbf{u}_h \in \mathscr{S}^h$ and $\tilde{p}_h \in \mathbf{P}^h$ solution of

$$\begin{aligned} a_{\mathtt{IP}}(\mathbf{u}_h,\mathbf{v})+c(\mathbf{u}_h;\mathbf{u}_h,\mathbf{v})+(\tilde{p}_h,[\![\mathbf{n}\cdot\mathbf{v}]\!])_{\Gamma\cup\Gamma_{\mathrm{D}}} &= l_{\mathtt{IP}}(\mathbf{v}) \quad \forall \mathbf{v}\in\mathscr{S}^h \\ (\tilde{q},[\![\mathbf{n}\cdot\mathbf{u}_h]\!])_{\Gamma\cup\Gamma_{\mathrm{D}}} &= (\tilde{q},\mathbf{n}\cdot\mathbf{u}_{\mathrm{D}})_{\Gamma_{\mathrm{D}}} \quad \forall \tilde{q}\in\mathbf{P}^h \end{aligned} \tag{9}$$

with the forms defined in (3) and (4).

The space of hybrid pressures (pressures along the sides in 2D or faces in 3D) is simply:

$$\mathbf{P}^h := \{\tilde{p} \mid \tilde{p}:\Gamma\cup\Gamma_{\mathrm{D}} \longrightarrow \mathbb{R} \text{ and } \tilde{p}=[\![\mathbf{n}\cdot\mathbf{v}]\!] \text{ for some } \mathbf{v}\in\mathscr{S}^h\} \tag{10}$$

In fact, Reference [2] demonstrates that $\mathbf{P}^h$ corresponds to piecewise polynomial pressures in the element sides in 2D or faces in 3D.

The second problem, which requires the solution of the previous one, evaluates the 'interior' pressures: find $p_h \in \mathscr{Q}^h$ such that

$$b(\mathbf{v},p_h)=l_{\mathtt{IP}}(\mathbf{v})-a_{\mathtt{IP}}(\mathbf{u}_h,\mathbf{v})-(\tilde{p}_h,[\![\mathbf{n}\cdot\mathbf{v}]\!])_{\Gamma\cup\Gamma_{\mathrm{D}}}-c(\mathbf{u}_h;\mathbf{u}_h,\mathbf{v}) \quad \forall \mathbf{v}\in\mathscr{J}^h \tag{11}$$

It is important to note that Equation (11) can be solved element-by-element and pressure is its only unknown.

Analogously, using the velocity space decomposition $\mathscr{V}^h=\mathscr{S}^h\oplus\mathscr{J}^h$, the CDG scheme proposed in (6) is also split into two uncoupled problems. For instance, the first problem for CDG is: find $\mathbf{u}_h\in\mathscr{S}^h$ and $\tilde{p}_h\in\mathbf{P}^h$ solution of

$$\begin{aligned} a_{\mathtt{CDG}}(\mathbf{u}_h,\mathbf{v})+c(\mathbf{u}_h;\mathbf{u}_h,\mathbf{v})+(\tilde{p}_h,[\![\mathbf{n}\cdot\mathbf{v}]\!])_{\Gamma\cup\Gamma_{\mathrm{D}}} &= l_{\mathtt{CDG}}(\mathbf{v}) \quad \forall \mathbf{v}\in\mathscr{S}^h \\ (\tilde{q},[\![\mathbf{n}\cdot\mathbf{u}_h]\!])_{\Gamma\cup\Gamma_{\mathrm{D}}} &= (\tilde{q},\mathbf{n}\cdot\mathbf{u}_{\mathrm{D}})_{\Gamma_{\mathrm{D}}} \quad \forall \tilde{q}\in\mathbf{P}^h \end{aligned} \tag{12}$$

with the forms defined in (7).

A major advantage of solenoidal spaces is the reduction in the number of dof for the DG solution. Table I and Figure 2 show the number of dof for a typical finite element mesh corresponding to a continuous Galerkin (cG) discretization, a DG nodal interpolation, and a DG solenoidal approximation (DGS).

Some hypotheses have been taken to obtain the formulas in Table I. For a typical kth-order cG finite element mesh, the number of nodes is approximated by $\frac{1}{2}k^2\mathtt{n_{el}}$ in 2D, and $\frac{1}{6}k^3\mathtt{n_{el}}$ in 3D, where $\mathtt{n_{el}}$ is the number of elements. In addition, note that for cG and DG, the number of dof for velocities and interior pressures is contemplated, whereas for the DGS approximation the number of dof for velocities and hybrid pressures is considered. In this case, in order to count the dof for hybrid pressures, the number of sides in a 2D finite element mesh is approximated by $\frac{3}{2}\mathtt{n_{el}}$, and the number of faces in a 3D mesh is approximated by $2\mathtt{n_{el}}$.

DOI: 10.1002/fld

Table I. Comparison of total number of dof, divided by the number of elements, for a typical finite element mesh corresponding to a continuous Galerkin (cG) discretization, a DG nodal interpolation, and a DG solenoidal approximation, with order k for velocity and $k-1$ for pressure, in 2D and 3D.

	2D	3D
cG	$\frac{3}{2}k^2+\frac{1}{2}k$	$\frac{2}{3}k^3+\frac{1}{2}k^2+\frac{1}{3}k$
DG	$\frac{3}{2}k^2+\frac{7}{2}k+2$	$\frac{2}{3}k^3+\frac{7}{2}k^2+\frac{35}{6}k+3$
DGS	$\frac{1}{2}k^2+4k+2$	$\frac{1}{3}k^3+\frac{7}{2}k^2+\frac{37}{6}k+3$

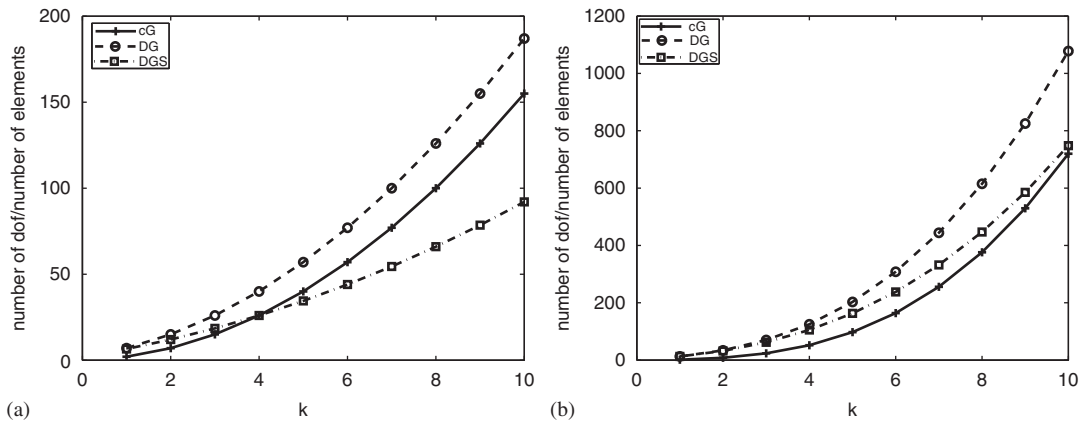

Figure 2. Comparison of the total number of dof, divided by the number of elements, for a typical finite element mesh corresponding to a continuous Galerkin (cG) discretization, a DG nodal interpolation, and a DG solenoidal approximation (DGS), in 2D (a) and 3D (b), with order k for velocity and $k-1$ for pressure.

Figure 2 shows the important reduction in dof when using a solenoidal approximation with hybrid pressures in a DG formulation. Moreover, compared with cG, the DGS approximation leads to less dof in 2D, and to a competitive number of dof in 3D. From the formulas giving the number of dof in Table I, other conclusions can also be derived. The coefficient of the leading term in the dof formula is the same for cG and standard DG, and it is greater than the corresponding coefficient for solenoidal DG. Thus, cG and standard DG behave similarly when increasing k, whereas the growth of the number of dof of the solenoidal DG method is much slower.

It is worth mentioning that an additional reduction in the number of dof can be achieved introducing a non-consistent penalty parameter to weakly enforce continuity of normal velocities along element sides/faces. Following the rationale in [6], alternative DG formulations can be derived, where the computation of velocity and pressure is completely decoupled, with an apparent reduction in computational cost. Nevertheless, as usual in non-consistent penalty formulations, it may lead to ill-conditioned systems of equations, see [6] for details.

DOI: 10.1002/fld

3. NUMERICAL EXAMPLES

IPM and CDG with solenoidal approximation are compared for the steady incompressible Navier–Stokes equations in this section. In all examples, a structured mesh of triangles is used, with interpolation of order k and $k-1$ for velocity and pressure, respectively.

3.1. Condition number of the diffusion matrix

The influence of the C_{11} parameter on the condition number of the diffusion matrix—the discretization of the bilinear form $a_{\mathtt{CDG}}(\cdot,\cdot)$ for CDG or $a_{\mathtt{IP}}(\cdot,\cdot)$ for IPM—is studied next. Figure 3 shows the evolution of the condition number for a regular structured mesh with $h=\frac{1}{8}$ and degree $k=4$.

For $C_{11}\geqslant 40h^{-1}$, that is, for C_{11} large enough to ensure coercivity of the IPM bilinear form, similar condition numbers are obtained with both methods. Figure 3 also shows that CDG (and it would also be the case for LDG) allows to choose a value of C_{11} as small as wanted, see [8]. Nevertheless, the condition number is rather constant for small value of C_{11}, and the minimum value of the condition number is more or less the same for CDG and for IPM. Thus, the flexibility of CDG for the choice of C_{11} does not imply any advantage in front of IPM for the conditioning of the matrix.

3.2. Driven cavity example

A standard benchmark test for the Navier–Stokes equations is now considered. A plane flow of an isothermal fluid in a lid-driven cavity is modeled in a 2D square domain $\Omega=]0,1[\times]0,1[$, with zero body force and one moving wall. A continuous velocity

$$\mathbf{u}=\begin{cases}(10x,0)^{\mathrm{T}} & \text{for } 0\leqslant x\leqslant 0.1\\ (1,0)^{\mathrm{T}} & \text{for } 0.1\leqslant x\leqslant 0.9\\ (10-10x,0)^{\mathrm{T}} & \text{for } 0.9\leqslant x\leqslant 1\end{cases}$$

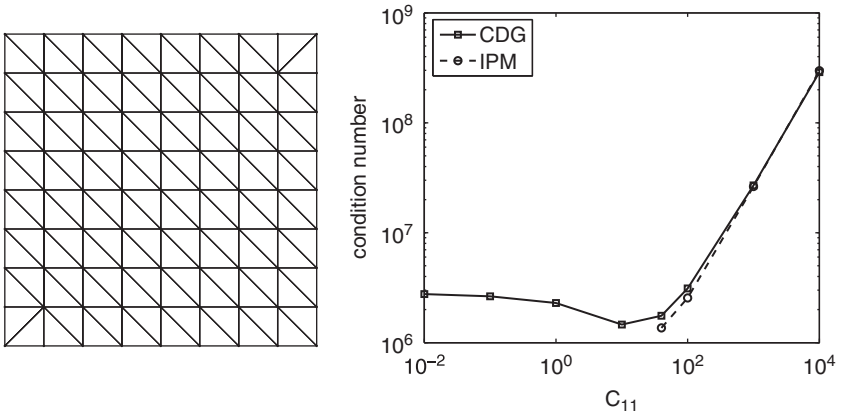

Figure 3. Structured mesh for $h=\frac{1}{8}$ and dependency of the condition number of the diffusion matrix on the stabilization parameter C_{11}, for CDG and IPM, with a fourth-order approximation of the velocity ($k=4$).

DOI: 10.1002/fld

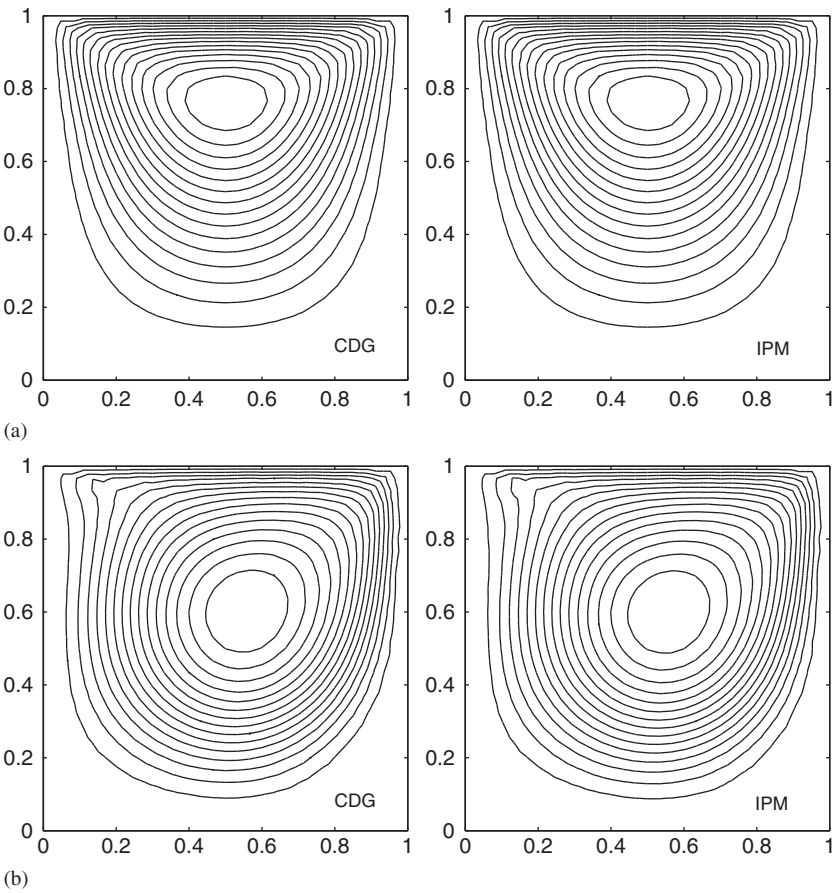

Figure 4. Velocity streamlines for CDG (left) and IPM (right) for $Re=1$ (a) and $Re=400$ (b), $k=2$, $h=0.0667$, $C_{11}=10h^{-1}$.

is imposed on the exterior upper boundary $\{y=1\}$, and a zero velocity $\mathbf{u}=(0,0)^{\mathrm{T}}$ is enforced on the three other sides.

Figure 4 shows the velocity streamlines, which fit to the expected solution. The main vortex moves toward the center of the cavity for increasing Reynolds number, both CDG and IPM giving very similar results. To further compare them, velocity profiles at the vertical centerline are shown in Figure 5 for $Re=1400$. First, it can be noticed that as the Reynolds number increases, the boundary layers are more obvious and the variations in the velocity are sharper. Second, results for CDG and IPM are again almost identical. To compare more precisely the accuracy of both methods, an analytical example is taken in the next section.

3.3. Analytical example

An example with analytical solution is considered next. The steady incompressible Navier–Stokes equations are solved in a 2D square domain $\Omega=]0,1[\times]0,1[$ with Dirichlet boundary conditions

DOI: 10.1002/fld

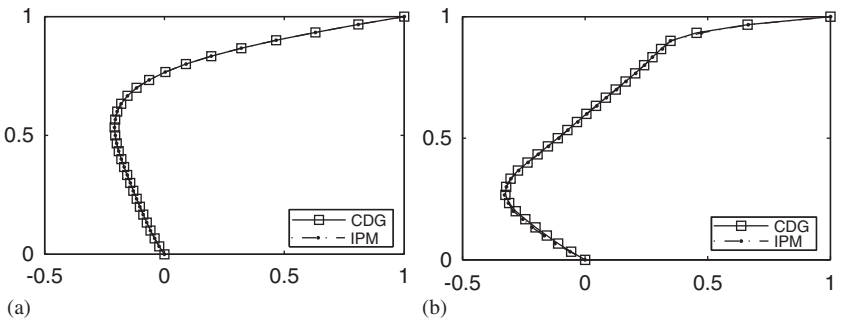

Figure 5. Velocity profiles at the vertical centerline for CDG and IPM for $Re=1$ (a) and $Re=400$ (b), $k=2$, $h=0.0667$, $C_{11}=10h^{-1}$.

on three sides and Neumann boundary condition on the fourth side $\{x=0\}$. A body force

$$\mathbf{f}=\begin{pmatrix} -4\nu(-1+2y)(y^2-6xy^2+6x^2y^2-y+6xy-6x^2y+3x^2-6x^3+3x^4) \\ \quad +1-2x+4x^3y^2(2y^2-2y+1)(y-1)^2(-1+2x)(x-1)^3 \\ 4\nu(-1+2x)(x^2-6x^2y+6x^2y^2-x+6xy-6xy^2+3y^2-6y^3+3y^4) \\ \quad +4x^2y^3(-1+2y)(y-1)^3(2x^2-2x+1)(x-1)^2 \end{pmatrix}$$

is imposed in order to have the polynomial exact solution

$$\mathbf{u}=\begin{pmatrix} x^2(1-x)^2(2y-6y^2+4y^3) \\ -y^2(1-y)^2(2x-6x^2+4x^3) \end{pmatrix}$$

$$p=x(1-x)$$

Fourth-order approximation for velocity and cubic approximation for pressure (i.e. $k=4$) are considered.

The influence of C_{11} on the accuracy of CDG is analyzed. Figure 6 shows the results for velocity, hybrid pressure, and interior pressure $\mathscr{L}_2$-errors with $hC_{11}=1, 10, 40$ and $C_{11}^*=0$, which denotes $C_{11}=0$ on interior faces and $C_{11}=h^{-1}$ on the Dirichlet boundary, see Remark 1. Optimal convergence is obtained in all cases, with similar accuracy, though larger values $C_{11}=10h^{-1}$ or $C_{11}=40h^{-1}$ give slightly worse results for velocity and hybrid pressure errors, but slightly better results for pressure error.

CDG and IPM are compared from an accuracy point of view in Figure 7. $C_{11}=40h^{-1}$ is considered for both methods. Note that, as seen in Figure 6, $C_{11}=40h^{-1}$ provides accurate results for CDG and it is also close to the minimum value that ensures coercivity of the IPM bilinear form. With this selection of C_{11}, similar results are obtained: both methods reach optimal convergence rates for velocity and hybrid pressure with similar accuracy.

DOI: 10.1002/fld

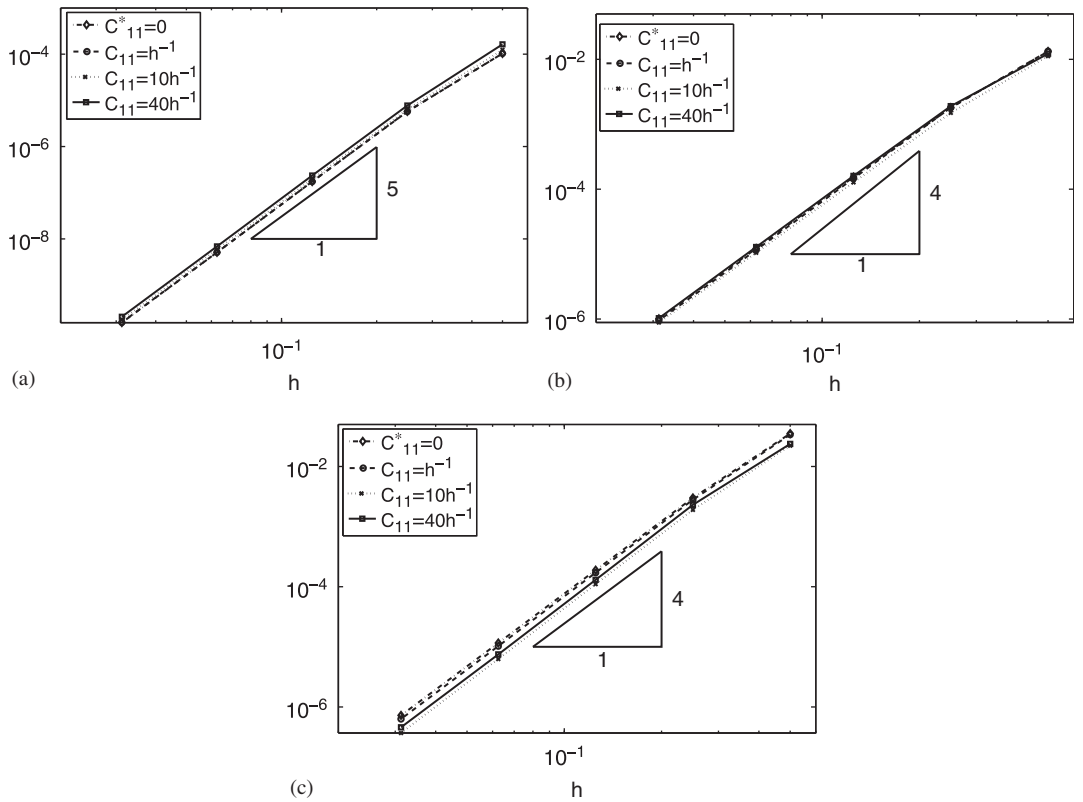

Figure 6. Comparison of $\mathscr{L}_2$-errors obtained with CDG for different values of C_{11}, for a fourth-order approximation of the velocity and a cubic interpolation of hybrid and interior pressures: (a) Velocity $\mathscr{L}_2$-error; (b) Hybrid pressure $\mathscr{L}_2$-error; (c) Interior pressure $\mathscr{L}_2$-error.

4. CONCLUSIONS

An IPM and a CDG formulation for solving the steady incompressible Navier–Stokes equations are proposed. Both methods can be easily applied using high-order piecewise divergence-free approximations, leading to two uncoupled problems: one for velocities and hybrid pressures, and one for an element-by-element computation of pressure in the interior of the elements.

Although both formulations are derived from different rationales, CDG can be written as the IPM formulation plus some extra terms, some of them related to lifting operators. These extra terms allow more flexibility in the choice of the C_{11} parameter, which can even be set as $C_{11}=0$ for all internal sides/faces in CDG, whereas it has to be taken big enough in the whole domain to ensure coercivity of the bilinear form of IPM.

Though the bilinear form of CDG introduces more terms, the stencil is the same in both methods, and both formulations present the major advantage—relative to LDG for example—that they are compact formulations: dof of one element are only connected to those of immediate neighbors.

DOI: 10.1002/fld

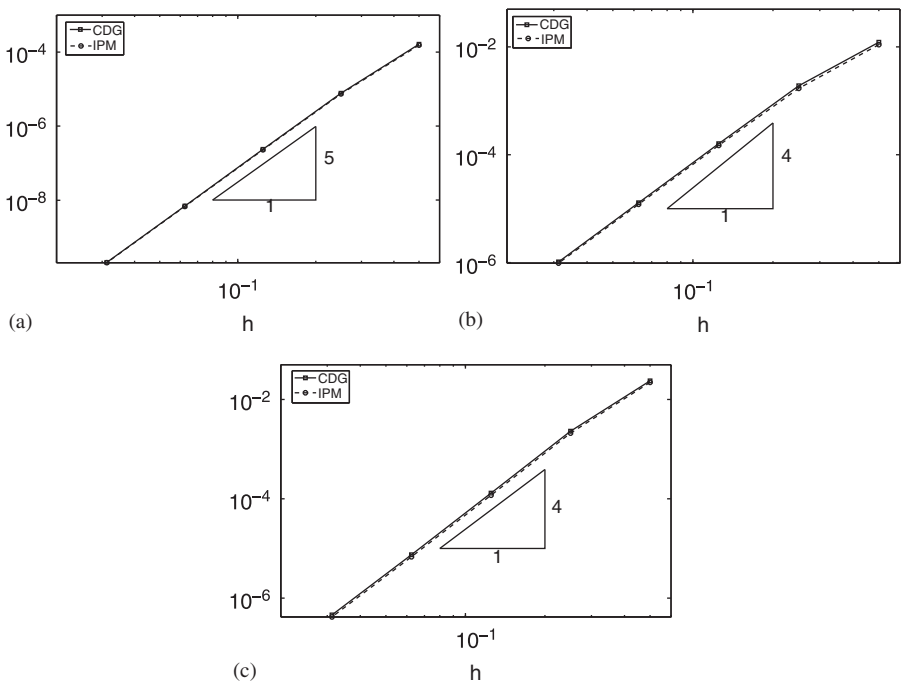

Figure 7. Comparison of $\mathscr{L}_2$-errors obtained with CDG and IPM for a fourth-order approximation of the velocity and a cubic interpolation of hybrid and interior pressures, with $C_{11}=40h^{-1}$: (a) Velocity $\mathscr{L}_2$-error; (b) Hybrid pressure $\mathscr{L}_2$-error; (c) Interior pressure $\mathscr{L}_2$-error.

Numerical experiments reveal that IPM and CDG present similar results for the condition number of the diffusion matrix, and for the accuracy of the numerical solution, both reaching optimal convergence rates for velocity and pressure.

Thus, the main differences between both methods are that CDG is less sensitive to the selection of the penalty parameter (tuning of C_{11} is almost eliminated), but it has the major disadvantage of the implementation and computation of the lifting operators. That is, IPM leads to a simpler and straightforward implementation, avoiding the extra computational cost associated with CDG or LDG liftings.

APPENDIX A: IMPLEMENTATION OF LIFTING OPERATORS

CDG introduces the concept of lifting operators, whose implementation is not trivial. As an example, the discretization of the lifting product $\int_\Omega r^e(\llbracket \mathbf{n}\otimes\mathbf{u}\rrbracket):r^e(\llbracket \mathbf{n}\otimes\mathbf{v}\rrbracket)\,\mathrm{d}\Omega$ in (7a) is commented next.

In the following, solenoidal vector functions are discretized in each element Ω_k (for $k=1,\ldots,\mathtt{n_{el}}$) with a solenoidal vector basis $\boldsymbol{\phi}_i^k$ (see Section 2.4) as

$$\mathbf{v}=\sum_{i=1}^{\mathtt{n_{bf}}}\boldsymbol{\phi}_i^k\mathrm{v}_i^k \quad \text{in } \Omega_k$$

DOI: 10.1002/fld

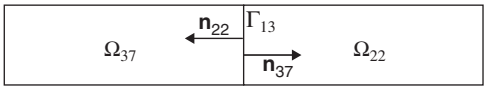

Figure A1. Elements Ω_{37} and Ω_{22} share face Γ_{13}; $\mathbf{n}_{37}$ and $\mathbf{n}_{22}$ are, respectively, exterior unit normals to Ω_{37} and Ω_{22}.

with some scalar coefficients v_i^k, where $\mathtt{n_{bf}}$ is the number of basis functions in each element. The solenoidal discrete space in Ω_k is denoted as $\mathscr{S}(\Omega_k) := <\boldsymbol{\phi}_i^k>_{i=1}^{\mathtt{n_{bf}}}$. The corresponding space of tensor functions is $\nabla^{\mathrm{s}}\mathscr{S}(\Omega_k)$, and therefore, a tensor $\boldsymbol{\tau} \in \nabla^{\mathrm{s}}\mathscr{S}(\Omega_k)$ will be expressed as $\boldsymbol{\tau} = \sum_{i=1}^{\mathtt{n_{tf}}} \boldsymbol{\psi}_i^k \boldsymbol{\tau}_i^k$ in Ω_k, with scalar coefficients $\boldsymbol{\tau}_i^k \in \mathbb{R}$, $\boldsymbol{\psi}_i^k \in \nabla^{\mathrm{s}}\mathscr{S}(\Omega_k)$ and $\mathtt{n_{tf}} = \dim\{\nabla^{\mathrm{s}}\mathscr{S}(\Omega_{\mathrm{k}})\}$. For instance, for $k=2$ a solenoidal basis is detailed in (8) and a tensor basis of $\nabla^{\mathrm{s}}\mathscr{S}(\Omega_k)$ is

$$\left\langle \begin{pmatrix} 0 & \frac{1}{2} \\ \frac{1}{2} & 0 \end{pmatrix}, \begin{pmatrix} 1 & 0 \\ 0 & -1 \end{pmatrix}, \begin{pmatrix} 0 & x \\ x & 0 \end{pmatrix}, \begin{pmatrix} 2y & x \\ x & -2y \end{pmatrix}, \begin{pmatrix} 2x & -y \\ -y & -2x \end{pmatrix}, \begin{pmatrix} 0 & y \\ y & 0 \end{pmatrix} \right\rangle$$

Moreover, for every side Γ_e, or face in 3D, $\ell(e,1)$ and $\ell(e,2)$, respectively, denote the numbers of the first element (left element) and the second element (right element) sharing the side. Figure A1 shows an example where side Γ_{13} is shared by elements Ω_{37} and Ω_{22}, thus for this side $\ell(13,1)=37$ and $\ell(13,2)=22$.

In CDG, lifting terms are implemented with a loop in sides (faces in 3D). Thus, let us consider a side $\Gamma_e = \overline{\Omega}_{\ell(e,1)} \cap \overline{\Omega}_{\ell(e,2)}$. The lifting operator associated with side Γ_e, r^e, is zero outside $\Omega_{\ell(e,1)} \cup \Omega_{\ell(e,2)}$. Thus, the lifting term appearing in the bilinear form can be expressed as a sum of integrals in $\Omega_{\ell(e,1)}$ and $\Omega_{\ell(e,2)}$,

$$\int_\Omega r^e(\llbracket \mathbf{n} \otimes \mathbf{u} \rrbracket) : r^e(\llbracket \mathbf{n} \otimes \mathbf{v} \rrbracket)\, \mathrm{d}\Omega = \int_{\Omega_{\ell(e,1)}} r^e(\llbracket \mathbf{n} \otimes \mathbf{u} \rrbracket) : r^e(\llbracket \mathbf{n} \otimes \mathbf{v} \rrbracket)\, \mathrm{d}\Omega + \int_{\Omega_{\ell(e,2)}} r^e(\llbracket \mathbf{n} \otimes \mathbf{u} \rrbracket) : r^e(\llbracket \mathbf{n} \otimes \mathbf{v} \rrbracket)\, \mathrm{d}\Omega$$

requiring the computation of r^e only in $\Omega_{\ell(e,1)}$ and $\Omega_{\ell(e,2)}$. In fact, given the discontinuous nature of the test functions $\boldsymbol{\tau}$ in (5), the lifting can be computed separately in each one of the two elements. For instance, taking test functions $\boldsymbol{\tau}$ with support in $\Omega_{\ell(e,1)}$, first equation in (5) is particularized as

$$\int_{\Omega_{\ell(e,1)}} r^e(\llbracket \mathbf{n} \otimes \mathbf{u} \rrbracket) : \boldsymbol{\tau}\, \mathrm{d}\Omega = \frac{1}{2} \int_{\Gamma_e} \llbracket \mathbf{n} \otimes \mathbf{u} \rrbracket : \boldsymbol{\tau}\, \mathrm{d}\Gamma \quad \forall \boldsymbol{\tau} \in \nabla^{\mathrm{s}}\mathscr{S}(\Omega_{\ell(e,1)}) \tag{A1}$$

which can be interpreted as a formula for computing the lifting in the first element, that is, $r^e|_{\Omega_{\ell(e,1)}}$. Discretization of (A1) leads to the matrix equation

$$\mathbf{M}^{\Omega_{\ell(e,1)}} \mathbf{r}_{\mathbf{u}}^{e,1} = \mathbf{S}_{11}^e \mathbf{u}^{\ell(e,1)} + \mathbf{S}_{21}^e \mathbf{u}^{\ell(e,2)} \tag{A2}$$

where $\mathbf{u}^{\ell(e,1)}$ and $\mathbf{u}^{\ell(e,2)}$ are vectors containing the coefficients of the interpolation of $\mathbf{u}$ in $\Omega_{\ell(e,1)}$ and $\Omega_{\ell(e,2)}$, respectively, $\mathbf{r}_{\mathbf{u}}^{e,1}$ is a vector containing the coefficients corresponding to the lifting of $\llbracket \mathbf{n} \otimes \mathbf{u} \rrbracket$ in the first element, that is

$$r^e(\llbracket \mathbf{n} \otimes \mathbf{u} \rrbracket) = \sum_{i=1}^{\mathtt{n_{tf}}} \boldsymbol{\psi}_i^{\ell(e,1)} (\mathbf{r}_{\mathbf{u}}^{e,1})_i \quad \text{in } \Omega_{\ell(e,1)}$$

DOI: 10.1002/fld

and $\mathbf{M}^{\Omega_k}$ (for $k=1,\ldots,\mathtt{n_{el}}$) and $\mathbf{S}^e_{\alpha\beta}$ (for $\alpha,\beta=1,2$) are block matrices given by

$$[\mathbf{M}^{\Omega_k}]_{ij}=\int_{\Omega_k}\boldsymbol{\psi}_i^k:\boldsymbol{\psi}_j^k\,\mathrm{d}\Omega \quad \text{for } i,j=1\ldots\mathtt{n_{tf}}$$

$$[\mathbf{S}^e_{\alpha\beta}]_{ij}=\frac{1}{2}\int_{\Gamma_e}\boldsymbol{\psi}_i^{\ell(e,\beta)}:(\mathbf{n}_{\ell(e,\alpha)}\otimes\boldsymbol{\phi}_j^{\ell(e,\alpha)})\,\mathrm{d}\Gamma \quad \text{for } i=1\ldots\mathtt{n_{tf}} \quad \text{and } \mathtt{j}=1\ldots\mathtt{n_{bf}}$$

For illustration purposes, note that for the example in Figure A1, exterior normal vectors appearing in the definition of $\mathbf{S}^e_{\alpha\beta}$ are $\mathbf{n}_{\ell(e,1)}=\mathbf{n}_{37}$ and $\mathbf{n}_{\ell(e,2)}=\mathbf{n}_{22}$, that is, exterior unit normals to Ω_{37} and Ω_{22}, respectively.

Analogously, the lifting in $\Omega_{\ell(e,2)}$ is determined by

$$\mathbf{M}^{\Omega_{\ell(e,2)}}\mathbf{r}^{e,2}_{\mathbf{u}}=\mathbf{S}^e_{12}\mathbf{u}^{\ell(e,1)}+\mathbf{S}^e_{22}\mathbf{u}^{\ell(e,2)}$$

where $\mathbf{r}^{e,2}_{\mathbf{u}}$ is the vector containing the coefficients corresponding to the lifting $r^e(\llbracket\mathbf{n}\otimes\mathbf{u}\rrbracket)$ in $\Omega_{\ell(e,2)}$.

Now, using the discretization of the lifting (A2), the contribution of the first element $\Omega_{\ell(e,1)}$ to the lifting product appearing in the CDG weak form corresponds to

$$\begin{aligned}\int_{\Omega_{\ell(e,1)}} r^e(\llbracket\mathbf{n}\otimes\mathbf{v}\rrbracket):r^e(\llbracket\mathbf{n}\otimes\mathbf{u}\rrbracket)\,\mathrm{d}\Omega&=(\mathbf{r}^{e,1}_{\mathbf{v}})^{\mathrm{T}}\mathbf{M}^{\Omega_{\ell(e,1)}}\mathbf{r}^{e,1}_{\mathbf{u}}\\&=(\mathbf{S}^e_{11}\mathbf{v}^{\ell(e,1)}+\mathbf{S}^e_{21}\mathbf{v}^{\ell(e,2)})^{\mathrm{T}}(\mathbf{M}^{\Omega_{\ell(e,1)}})^{-1}(\mathbf{S}^e_{11}\mathbf{u}^{\ell(e,1)}+\mathbf{S}^e_{21}\mathbf{u}^{\ell(e,2)})\end{aligned}$$

Finally, following the same derivation for the second element and summing the contribution of both elements, the lifting product appearing in the CDG weak form for the eth side Γ_e corresponds to

$$\begin{aligned}\int_{\Omega} r^e(\llbracket\mathbf{n}\otimes\mathbf{v}\rrbracket):r^e(\llbracket\mathbf{n}\otimes\mathbf{u}\rrbracket)\,\mathrm{d}\Omega&=(\mathbf{v}^{\ell(e,1)})^{\mathrm{T}}\mathbf{K}^e_{11}\mathbf{u}^{\ell(e,1)}+(\mathbf{v}^{\ell(e,1)})^{\mathrm{T}}\mathbf{K}^e_{12}\mathbf{u}^{\ell(e,2)}\\&\quad+(\mathbf{v}^{\ell(e,2)})^{\mathrm{T}}\mathbf{K}^e_{22}\mathbf{u}^{\ell(e,2)}+(\mathbf{v}^{\ell(e,2)})^{\mathrm{T}}(\mathbf{K}^e_{12})^{\mathrm{T}}\mathbf{u}^{\ell(e,1)}\end{aligned}$$

with matrices given by

$$\mathbf{K}^e_{\alpha\beta}=(\mathbf{S}^e_{\alpha1})^{\mathrm{T}}(\mathbf{M}^{\Omega_{\ell(e,1)}})^{-1}\mathbf{S}^e_{\beta1}+(\mathbf{S}^e_{\alpha2})^{\mathrm{T}}(\mathbf{M}^{\Omega_{\ell(e,2)}})^{-1}\mathbf{S}^e_{\beta2}$$

for $\alpha,\beta=1,2$.

Thus, implementing a lifting term implies computing three matrices for each face Γ_e to be assembled in rows and columns corresponding to elements sharing this face, that is, elements (matrix blocks) with indexes $\ell(e,1)$ and $\ell(e,2)$.

Note that computing these matrices involves several elemental matrices, matrix inversions and products, with a clearly non-negligible increase in computational cost. Moreover, for unsteady problems solved with explicit time integrators, implementing the lifting also represents an important increase in computational cost: auxiliary variables for liftings have to be stored and computed (solving linear systems of equations in each element) at every time step.

REFERENCES

1. Cockburn B. Discontinuous Galerkin methods for computational fluid dynamics. *Encyclopedia of Computational Mechanics*, *vol. 3*: *Fluids*. Wiley: Chichester, 2004.

DOI: 10.1002/fld

2. Cockburn B, Gopalakrishnan J. Incompressible finite elements via hybridization. Part I: the Stokes system in two space dimensions. *SIAM Journal on Numerical Analysis* 2005; **43**(4):1627–1650.
3. Baker GA, Jureidini WN, Karakashian OA. Piecewise solenoidal vector fields and the Stokes problem. *SIAM Journal on Numerical Analysis* 1990; **27**(6):1466–1485.
4. Carrero J, Cockburn B, Schötzau D. Hybridized globally divergence-free LDG methods. Part I: the Stokes problem. *Mathematical Computation* 2005; **75**(254):533–563.
5. Hansbo P, Larson MG. Piecewise divergence-free discontinuous Galerkin methods for Stokes flow. *Communications in Numerical Methods in Engineering* 2008; **24**(5):355–366.
6. Montlaur A, Fernandez-Mendez S, Huerta A. Discontinuous Galerkin methods for the Stokes equations using divergence-free approximations. *International Journal for Numerical Methods in Fluids* 2008; **57**(9): 1071–1092.
7. Cockburn B, Kanschat G, Schötzau D. The local discontinuous Galerkin method for linearized incompressible fluid flow: a review. *Computers and Fluids* 2005; **34**:491–506.
8. Peraire J, Persson P-O. The compact discontinuous Galerkin (CDG) method for elliptic problems. *SIAM Journal on Scientific and Statistical Computation* 2008; **30**(4):1806–1824.
9. Arnold DN. An interior penalty finite element method with discontinuous elements. *SIAM Journal on Numerical Analysis* 1982; **19**(4):742–760.
10. Hansbo A, Hansbo P. A finite element method for the simulation of strong and weak discontinuities in solid mechanics. *Computer Methods in Applied Mechanics and Engineering* 2004; **193**(33–35):3523–3540.
11. Kanschat G, Schötzau D. Energy norm a posteriori error estimation for divergence-free discontinuous Galerkin approximations of the Navier–Stokes equations. *International Journal for Numerical Methods in Fluids* 2008; **57**(9):1093–1113.
12. Cockburn B, Kanschat G, Schötzau D. A locally conservative LDG method for the incompressible Navier–Stokes equations. *Mathematical Computation* 2005; **74**(251):1067–1095.
13. Cockburn B, Kanschat G, Perugia I, Schötzau D. Superconvergence of the local discontinuous Galerkin method for elliptic problems on cartesian grids. *SIAM Journal on Numerical Analysis* 2001; **39**(1):264–285.

DOI: 10.1002/fld